

# Supporting Information

H<sub>2</sub> Dissociation on H Precovered Ni(100)

Surface: Physisorbed State and Coverage

Dependence

*Ying He and Wenji Wang\**

College of Chemistry & Pharmacy, Northwest A&F University, Yangling, 712100,

Shaanxi Province, P. R. China.

\*Electronic address: [wjwang@nwafu.edu.cn](mailto:wjwang@nwafu.edu.cn)

## A. The Lattice Size Effect

The lattice model and the number of Ni atoms may affect the lattice motion effect on  $H_2$  dissociation. In order to investigate the lattice size effect, we prepare four lattice models, as seen in Figure S1. Lattice I is made up of 122 Ni atoms, and all of these Ni atoms are fixed. Lattice II also consists of 122 Ni atoms, but 11 (the red ones, surrounding the reaction path of  $H_2$ ) and 36 (the dark blue ones, close to the red ones) Ni atoms are treated as quantum and classical particles, respectively. Both Lattice III and IV are composed of 397 Ni atoms, while 11 and 36 Ni atoms in Lattice IV are treated quantum mechanically and classically, respectively. The calculated direct and steady state dissociation rates of  $H_2$  on these lattices have been listed in Table S1. The free energy profiles along the reaction path are displayed in Figure S2.

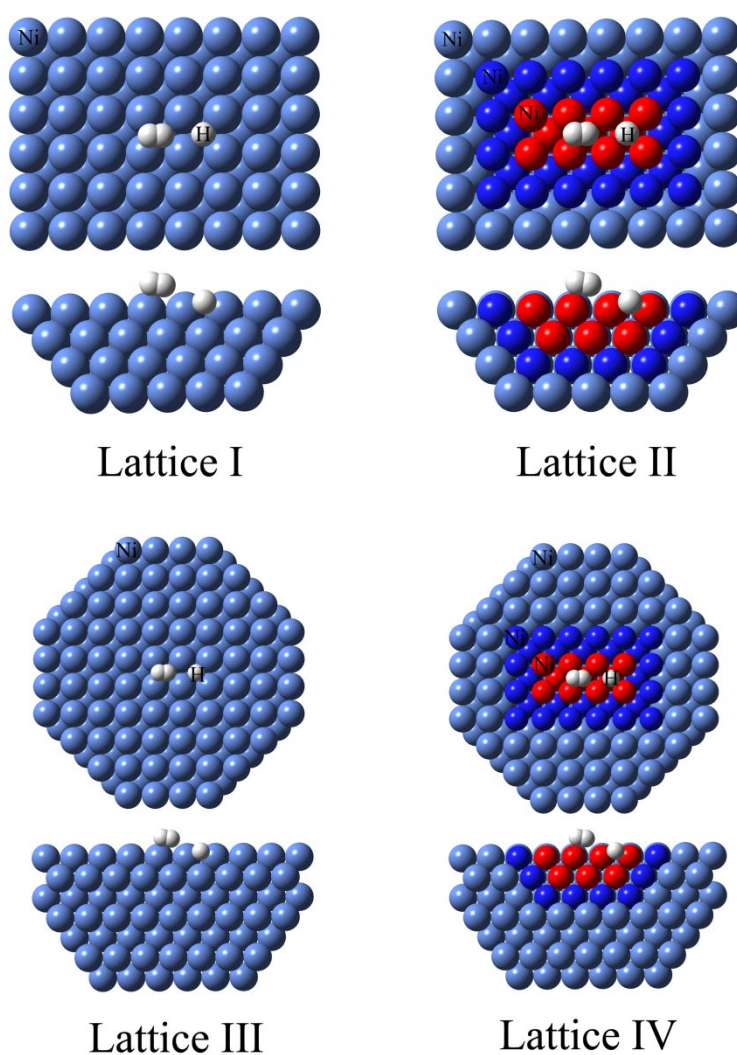


Figure S1. Plan and cross-sectional view of Ni(100) lattices. The grey balls represent H atoms. The red, dark blue, and light blue balls denote the nickel atoms treated quantum mechanically, classically, and rigidly, respectively.

Table S1. The Dissociation Rates ( $\text{cm}^3\cdot\text{site}^{-1}\cdot\text{s}^{-1}$ ) of  $\text{H}_2$  on H Precovered Ni(100)

		Lattice I	Lattice III	Lattice II	Lattice IV
300 K	direct	5.98(-13)	5.93(-13)	8.50(-13)	--- <sup>a</sup>
	steady state	1.03(-12)	1.07(-12)	1.42(-12)	---
600 K	direct	1.35(-12)	1.28(-12)	1.75(-12)	1.58(-12)
	steady state	6.26(-12)	5.97(-12)	7.90(-12)	7.42(-12)

<sup>a</sup> The value is not calculated because it is very time consuming.

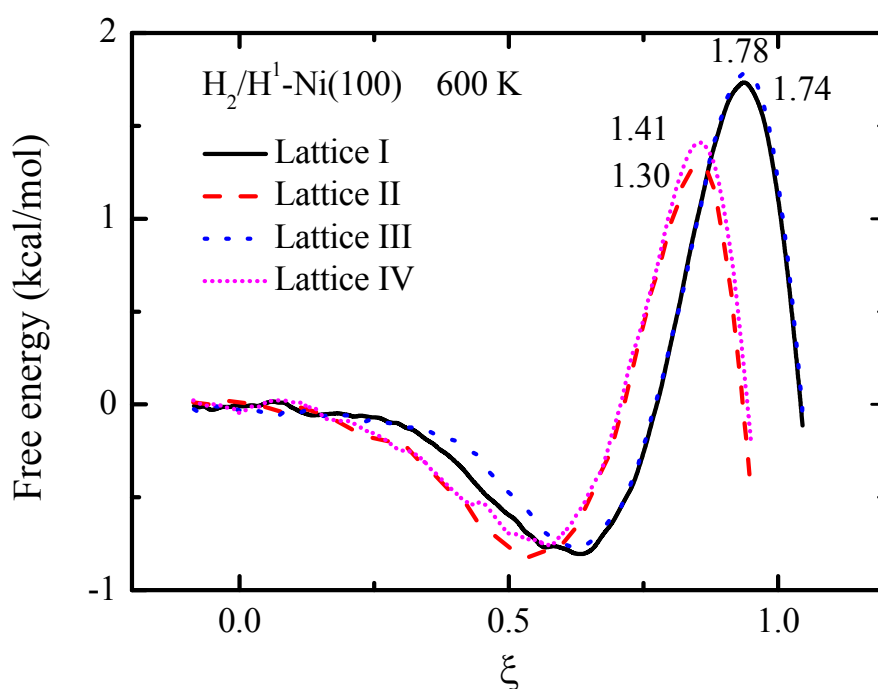


Figure S2. Free energy profiles along the reaction path for  $\text{H}_2$  dissociation on Lattice I, II, III and IV at 600 K.

In Table S1, we can see that the direct dissociation rates (as well as the steady state rates) of  $\text{H}_2$  on Lattice I and Lattice III are close to each other. We can also see from Figure S2 that the total free energy barrier on Lattice III is slightly higher than that on Lattice I by 0.04 kcal/mol at 600 K. These situations demonstrate that Lattice I is large enough to give converged rates on the rigid lattice. So, we chose Lattice I as the rigid lattice to calculate the rate constants.

On the quantum lattices, the direct dissociation rate of  $\text{H}_2$  on Lattice II is larger than that on Lattice IV by 11% at 600 K. It is also seen from Figure S2 that the total free energy barrier on Lattice IV is higher than that on Lattice II by 0.11 kcal/mol at 600 K. These phenomena reveal that Lattice IV is better than Lattice II to predict the lattice motion effect. However, the calculations on Lattice IV are very time consuming. For instance, with 20 cores, it costs 108 hours to simulate 1,000,000

Monte Carlo cycles at 600 K on Lattice IV. In particular, it reaches 230 hours to simulate 1,000,000 Monte Carlo cycles at 300 K. In fact, we usually need more than 4 million Monte Carlo cycles to obtain a converged ensemble average. So, it is hard to afford the computing time for the simulations on Lattice IV. Considering that Lattice IV does not improve the rates too much, and the computing time has a dramatic increase, we finally chose Lattice II as the quantum lattice to calculate the rate constants.

## B. The Preexponential Factor and Activation Energy

We have fitted our rate constants to the Arrhenius form (as seen in Figure S3(a-l)),

$$k(T) = A \cdot \exp\left(-\frac{E_a}{RT}\right)$$

where  $R$  is the gas constant,  $T$  is the temperature,  $A$  and  $E_a$  are the preexponential factor and activation energy, respectively. The obtained  $A$  and  $E_a$  for different processes are listed in Table S2 and S3.

Table S2. The Preexponential Factors ( $\text{cm}^3\cdot\text{site}^{-1}\cdot\text{s}^{-1}$ ) and Activation Energies (kcal/mol) for the Dissociation of  $\text{H}_2$

		250-400 K		400-800 K	
		$A$	$E_a$	$A$	$E_a$
$\text{H}_2/\text{Ni}(100)$	direct	5.43(-13)	-0.67	6.59(-12)	1.34
	rigid	3.33(-11)	1.45	1.89(-10)	2.92
$\text{H}_2/\text{H}^1\text{-Ni}(100)$	direct	8.10(-13)	0.13	4.80(-12)	1.52
	rigid	1.33(-11)	1.51	9.51(-11)	3.14
$\text{H}_2/\text{H}^1\text{-Ni}(100)$	direct	8.74(-13)	-0.04	6.11(-12)	1.50
	quantum	1.44(-11)	1.38	9.19(-11)	2.74
$\text{H}_2/\text{H}^2\text{-Ni}(100)$	direct	6.99(-13)	0.27	4.30(-12)	1.69
	rigid	9.80(-12)	1.51	7.76(-11)	3.19
$\text{D}_2/\text{D}^1\text{-Ni}(100)$	direct	8.06(-13)	1.04	4.10(-12)	2.53
	rigid	6.72(-12)	1.81	8.53(-11)	3.86
$\text{D}_2/\text{D}^1\text{-Ni}(100)$	direct	9.44(-13)	0.82	5.64(-12)	2.28
	quantum	8.76(-12)	1.65	9.55(-11)	3.59

Table S3. The Preexponential Factors ( $\text{s}^{-1}$ ) and Activation Energies (kcal/mol) for the Recombination of  $\text{H}_2$

		250-800 K	
		$A$	$E_a$
$\text{H}_2/\text{Ni}(100)$	rigid	2.69(14)	20.15
$\text{H}_2/\text{H}^1\text{-Ni}(100)$	rigid	2.36(14)	20.43
$\text{H}_2/\text{H}^1\text{-Ni}(100)$	quantum	2.03(14)	20.90
$\text{D}_2/\text{D}^1\text{-Ni}(100)$	rigid	2.27(14)	20.36
$\text{D}_2/\text{D}^1\text{-Ni}(100)$	quantum	1.99(14)	20.79

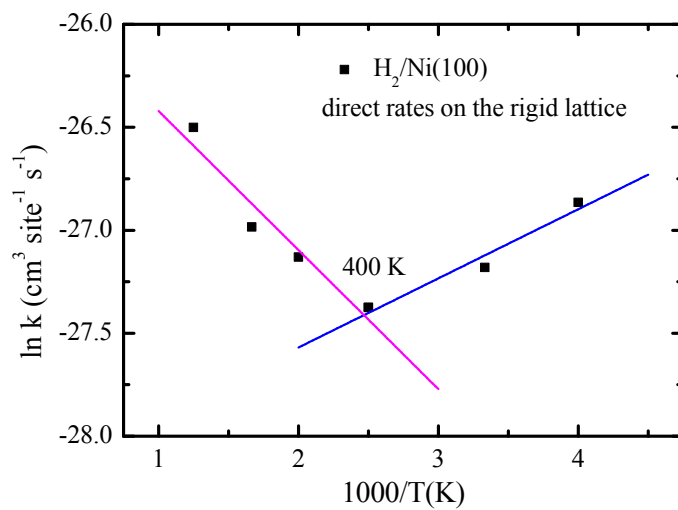


Figure S3(a). Fitting the direct rates of  $\text{H}_2/\text{Ni}(100)$  to the Arrhenius form.

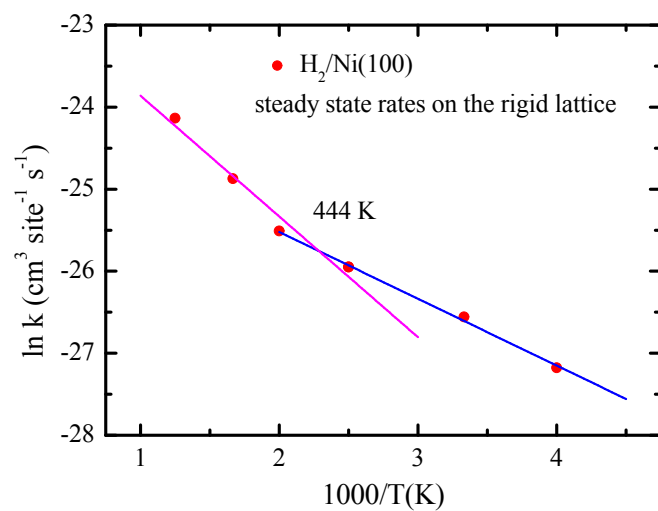


Figure S3(b). Fitting the steady state rates of  $\text{H}_2/\text{Ni}(100)$  to the Arrhenius form.

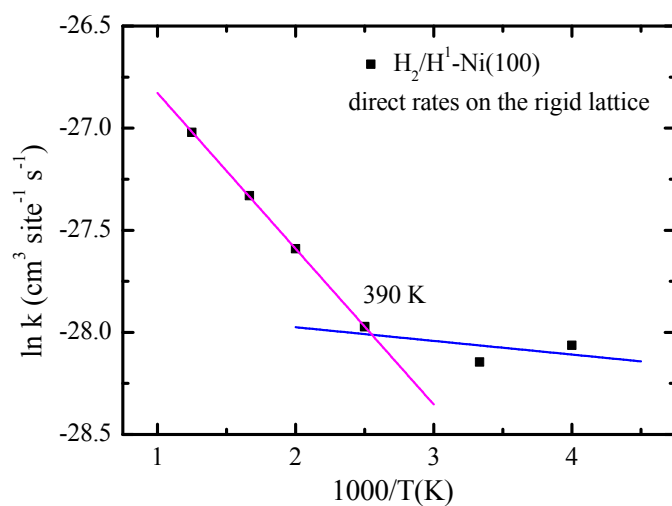


Figure S3(c). Fitting the direct rates of  $\text{H}_2/\text{H}^1$ -Ni(100) on the rigid lattice to the Arrhenius form.

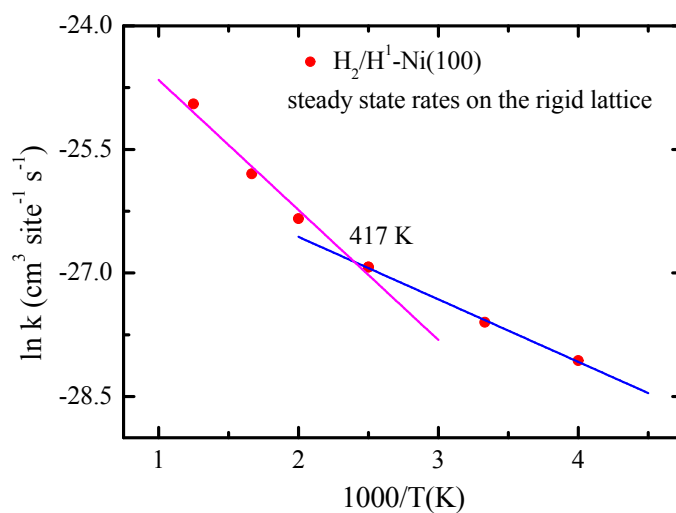


Figure S3(d). Fitting the steady state rates of  $\text{H}_2/\text{H}^1$ -Ni(100) on the rigid lattice to the Arrhenius form.

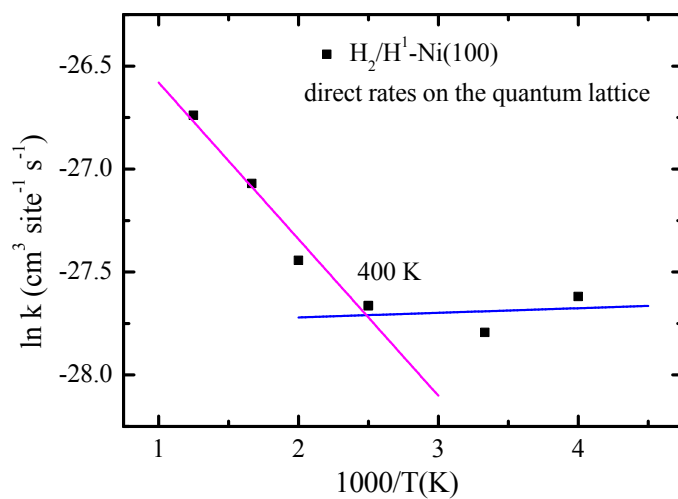


Figure S3(e). Fitting the direct rates of  $\text{H}_2/\text{H}^1\text{-Ni}(100)$  on the quantum lattice to the Arrhenius form.

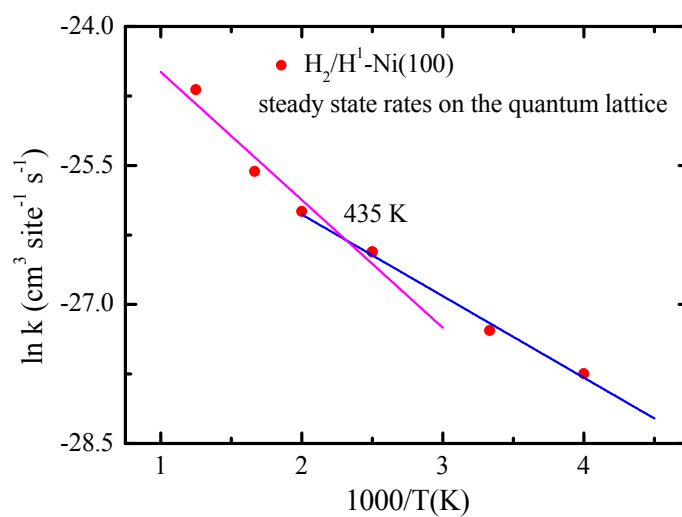


Figure S3(f). Fitting the steady state rates of  $\text{H}_2/\text{H}^1\text{-Ni}(100)$  on the quantum lattice to the Arrhenius form.

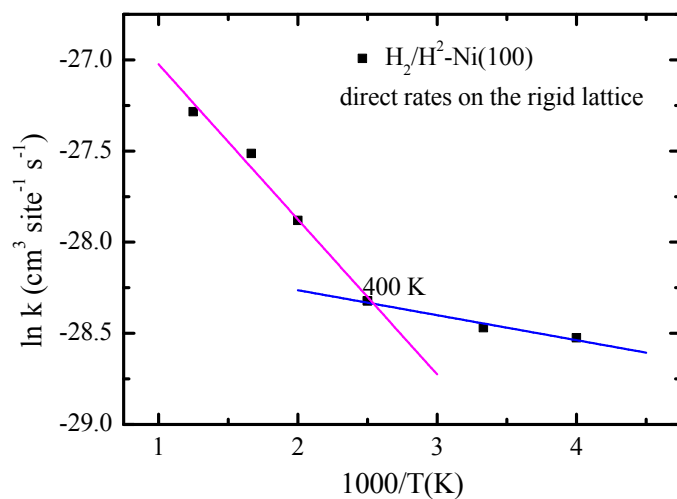


Figure S3(g). Fitting the direct rates of  $\text{H}_2/\text{H}^2$ -Ni(100) on the rigid lattice to the Arrhenius form.

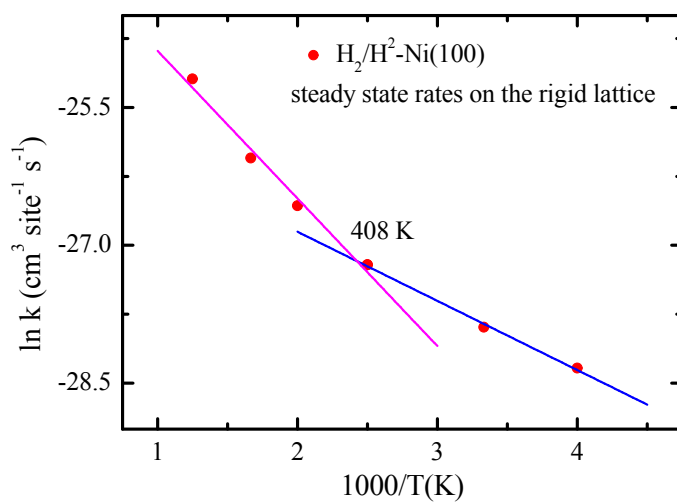


Figure S3(h). Fitting the steady state rates of  $\text{H}_2/\text{H}^2$ -Ni(100) on the rigid lattice to the Arrhenius form.

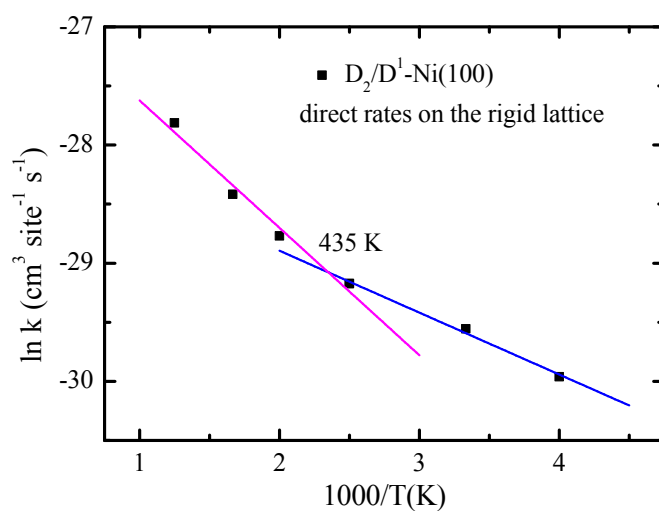


Figure S3(i). Fitting the direct rates of  $\text{D}_2/\text{D}^1$ -Ni(100) on the rigid lattice to the Arrhenius form.

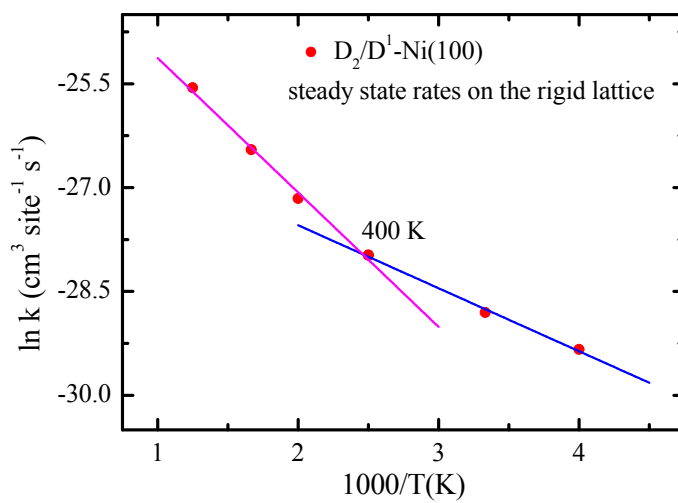


Figure S3(j). Fitting the steady state rates of  $\text{D}_2/\text{D}^1$ -Ni(100) on the rigid lattice to the Arrhenius form.

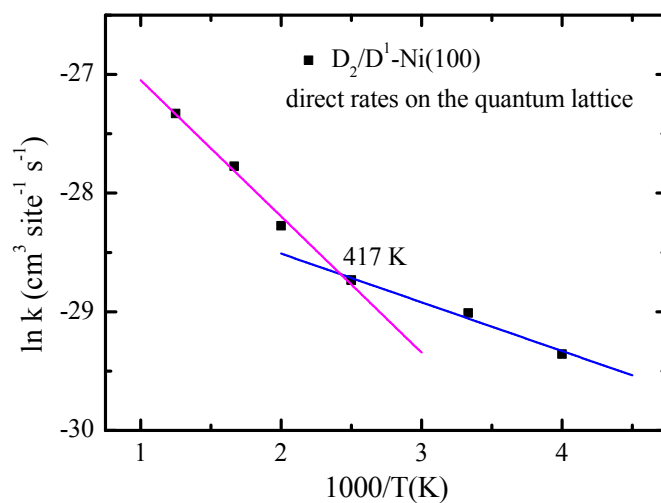


Figure S3(k). Fitting the direct rates of  $\text{D}_2/\text{D}^1$ -Ni(100) on the quantum lattice to the Arrhenius form.

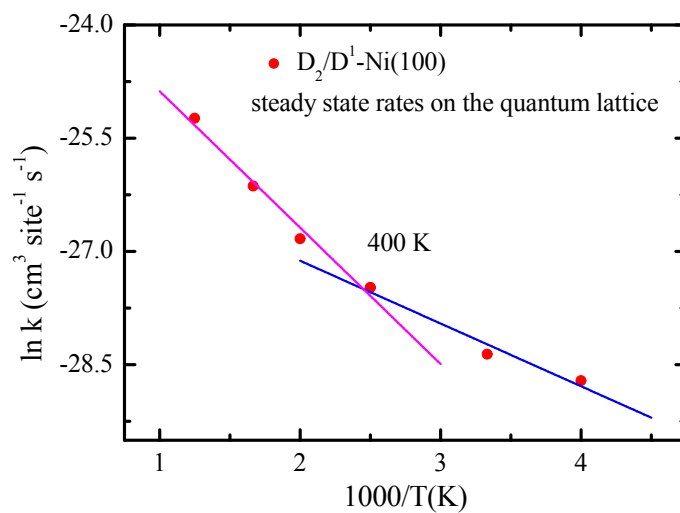


Figure S3(l). Fitting the steady state rates of  $\text{D}_2/\text{D}^1$ -Ni(100) on the quantum lattice to the Arrhenius form.